

Efficient temperature-dependent Green's functions methods for realistic systems: compact grids for orthogonal polynomial transforms

Alexei A. Kananenka, Jordan J. Phillips, and Dominika Zgid

Department of Chemistry, University of Michigan, Ann Arbor, Michigan 48109, United States

The temperature-dependent Matsubara Green's function that is used to describe temperature-dependent behavior is expressed on a numerical grid. While such a grid usually has a couple of hundred points for low-energy model systems, for realistic systems in large basis sets the size of an accurate grid can be tens of thousands of points, constituting a severe computational and memory bottleneck. In this paper, we determine efficient imaginary time grids for the temperature-dependent Matsubara Green's function formalism that can be used for calculations on realistic systems. We show that due to the use of orthogonal polynomial transform, we can restrict the imaginary time grid to few hundred points and reach micro-Hartree accuracy in the electronic energy evaluation. Moreover, we show that only a limited number of orthogonal polynomial expansion coefficients are necessary to preserve accuracy when working with a dual representation of Green's function or self-energy and transforming between the imaginary time and Matsubara frequency domain.

I. INTRODUCTION

The use of numerical grids in calculations for realistic systems has a long history in quantum chemistry simulations. For example, in density functional theory (DFT) a numerical integration is necessary for the evaluation of the exchange-correlation contribution to the density functional¹⁻⁵. Similarly, in Laplace transformed MP2 (LT-MP2) a quadrature is used to represent an integral that leads to the removal of the energy denominators⁶⁻¹¹. Recently, an implementation of random phase approximation (RPA)¹² appeared that uses an efficient imaginary time grid to yield temperature-independent RPA energy. The above mentioned methods are just a few examples of using efficient quadrature, a more extensive literature on the subject can be found in refs 13-32. Thus, it is fair to say that extensive knowledge exist on representing temperature-independent quantities on a grid when ground state methods are used. However, very little is known about how to efficiently represent temperature-dependent data on finite-temperature imaginary axis Matsubara grids.

Several factors distinguish the finite temperature Green's function from the zero-temperature Green's function formalism. Firstly, let us note that the temperature-dependent Green's function is a discrete object for which the grid points $i\omega_n$ are spaced according to the Matsubara grid $w_n = (2n + 1)\pi/\beta$, where $n \in \mathbb{Z}$ and $\beta = 1/k_B T$ is the inverse temperature. In comparison, the zero-temperature Green's function represented on imaginary axis is a continuous function. Similarly, the temperature-dependent imaginary time Green's function is an antiperiodic function between 0 and β , while the zero-temperature Green's function of imaginary time is a non-periodic function decaying rapidly and smoothly to zero. Consequently, traditional quadratures developed for zero-temperature RPA Green's functions used in ref 12 or LT-MP2 to represent denominators⁶ are not suitable for temperature-dependent Green's function calculations.

Currently, temperature-dependent Green's function calculations are mostly done for low-energy model systems. While such calculations for large realistic systems are still in their infancy, one can easily imagine that they could be very important in materials science for materials with small band gaps where the change of properties with temperature is significant and multiple states can be easily populated, or for a system which exhibit temperature-dependent phase transition caused by the electronic degrees of freedom.

Unlike the low-energy models, the orbital energies in realistic systems span a huge energy window frequently varying even between -3000 eV to 300 eV, see Figure 1. Thus, when quantitative accuracy in the calculations of realistic systems is desired, new challenges arise that are not present in model system calculations.

The temperature-dependent Green's functions have to be represented on a numerical grid with a spacing defined by the temperature but covering the energy window spanned by the realistic system. This usually results in a grid containing thousands of frequencies. Consequently, the Fourier transform from the imaginary time to the imaginary frequency axis, according to Nyquist theorem, requires twice as many imaginary time points as frequency points to yield accurate results. Having several thousands data points makes the calculations for realistic systems extremely challenging even if each grid point can be calculated in parallel.

Motivated by the aforementioned challenges, we first determine how the imaginary time grid can be truncated to a reasonable size and how the resulting errors can be controlled. To achieve it, we replace the numerical Fourier transform ($i\tau \rightarrow i\omega$) with an orthogonal polynomial transform ($i\tau \rightarrow L$) and ($L \rightarrow i\omega$), where as L we denote expansion coefficients of a Green's function or self-energy in an orthogonal polynomial basis. Subsequently, we examine if (i) the expansion coefficients L can be produced using a smaller number of grid points than currently used in the numerical Fourier transform, and if (ii) the number of expansion coefficients L is small

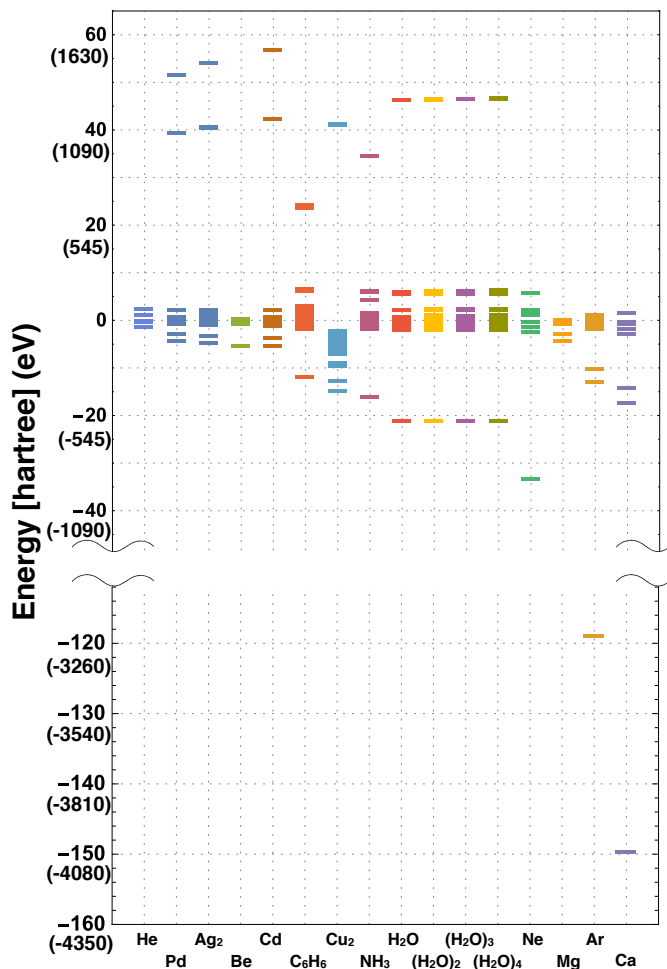


FIG. 1. Orbital energies for atoms and molecules in large basis sets containing diffuse orbitals.

enough that they can be easily stored in realistic calculations.

This paper is organized as follows. In section II, we review the necessary theoretical background leading to compact imaginary time grids and orthogonal polynomial transforms ($i\tau \rightarrow L \rightarrow i\omega$) using Legendre expansion coefficients. In section III, we discuss how an orthogonal polynomial transform can be used in the second order iterative Green’s function method (GF2) to reduce the size of the imaginary time grid. In section IV, we present numerical results showing that the required number of imaginary time points is much smaller than in the original uniform and power-law grid and that the number of required expansion coefficients can be kept small even if the micro-Hartree (μHa) accuracy is desired. Finally, we present conclusions in section V.

II. THEORY

In many Green’s function methods two Green’s function (G) or self-energy (Σ) representations are used: an imaginary time representation $G(i\tau)$ or $\Sigma(i\tau)$ and imaginary frequency representation $G(i\omega)$ or $\Sigma(i\omega)$. In an efficient implementation, one frequently changes from $i\tau$ to $i\omega$ and back, depending if it is more computationally advantageous to work with a $i\tau$ or $i\omega$ representation. Note that while the above statement is general and the $i\tau$ to $i\omega$ transform may be present in temperature-independent calculations such as RPA or GW^{12,33,34}, in this paper we focus exclusively on the imaginary time and frequency used for temperature-dependent Green’s functions^{35–38}.

Thus, frequently a Green’s function method proceeds according to scheme illustrated in Figure 2 and the computational bottleneck lies in the evaluation of $\Sigma(i\tau)$.

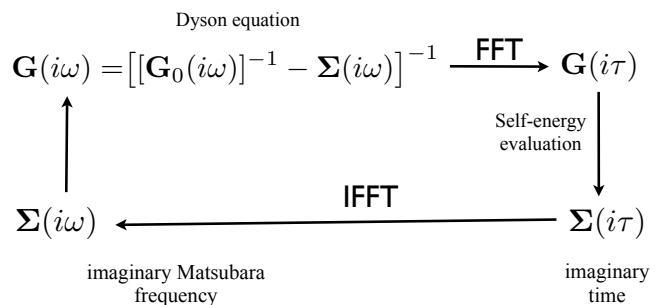


FIG. 2. An example of the representation change between imaginary time and frequency in Green’s functions methods. We denote the non-interacting and interacting/correlated Green’s functions as $G_0(i\omega)$ and $G(i\omega)$, respectively.

The number of imaginary time points used to represent $\Sigma(i\tau)$ enters as a prefactor. However, a sizable prefactor makes such calculations for large system impossible.

There are two reasons for the large size of imaginary time grids for temperature-dependent Green’s functions, firstly enough points are required to preserve the temperature dependence, secondly a significant number of points is required to make a numerical Fourier transform accurate.

A. Orthogonal polynomial representation of self-energy

We consider a single-particle temperature-dependent imaginary time self-energy $\Sigma(i\tau)$ on the interval $[0, \beta]$. The self-energy can be expanded in Legendre–Fourier series using orthogonal polynomials P_l . Note that different orthogonal polynomials, e.g. Chebyshev or Legendre, can be used as a basis. However, all results presented here should be valid regardless of the representation^{39,40}. In this work, we use Legendre polynomials defined on the interval $[-1, 1]$. The Legendre polynomial expansion of

the self-energy on this interval is given by

$$\Sigma_{ij}(i\tau) = \sum_{l \geq 0}^{\infty} \frac{\sqrt{2l+1}}{\beta} P_l(x(i\tau)) \Sigma_{ij}^l, \quad (1)$$

where $P_l(x(i\tau))$ is a Legendre polynomial of rank l and Σ_{ij}^l is the corresponding expansion coefficient,

$$\Sigma_{ij}^l = \sqrt{2l+1} \int_0^{\beta} d\tau P_l(x(\tau)) \Sigma_{ij}(i\tau), \quad (2)$$

and $x(\tau) = 2\tau/\beta - 1$ maps interval $[0, \beta]$ onto $[-1, 1]$. For detailed description of the properties of Legendre polynomials see ref 41.

In the past, several advantages of using an orthogonal polynomial representation of Green's function (and self-energy) were explored. Boehnke et. al.³⁹ used the Legendre polynomial representation of Green's functions as a noise filter in continuous-time hybridization expansion quantum Monte Carlo (CT-HYB) calculations. Additionally, the Legendre representation of Green's function can be more compact than Matsubara Green's function^{39,42,43}.

In this paper, we describe another advantage of using Legendre representation. It allows us to perform an orthogonal polynomial two step transform ($\Sigma(i\tau) \rightarrow L$) and ($L \rightarrow \Sigma(i\omega)$) and to reduce the size of the imaginary time grid that would be otherwise necessary to maintain a high accuracy. This ($\Sigma(i\tau) \leftrightarrow L$) transformation is unitary and can be written as a matrix multiplication

$$\begin{aligned} \Sigma_{ij}(i\omega_n) &= \sum_{l \geq 0}^{\infty} \Sigma_{ij}^l \frac{\sqrt{2l+1}}{\beta} \int_0^{\beta} d\tau e^{i\omega_n \tau} P_l(x(\tau)) \\ &= \sum_{l \geq 0}^{\infty} T_{nl} \Sigma_{ij}^l, \end{aligned} \quad (3)$$

where T_{nl} is the unitary matrix with elements defined as

$$T_{nl} = (-1)^n i^{l+1} \sqrt{2l+1} j_l \left(\frac{(2n+1)\pi}{2} \right), \quad (4)$$

where $j_l(z)$ are the spherical Bessel functions of the second kind.

Even though the Legendre series is infinite in principle, in all practical calculations only a finite number of expansion coefficients is used. For all atomic and molecular systems studied here the expansion coefficients decay very fast. In the worst case, only a few hundreds of them are necessary (see section IV), therefore only $O(N_l n^2)$ double precision numbers have to be stored, where n is the number of orbitals and N_l is the number of terms in the Legendre expansion. In contrast to calculations employing orthogonal polynomial transform, a typical numerical Fourier transform may require tens to hundreds of thousands of imaginary time grid points N_{τ} , making the cost of evaluation of the self-energy very significant.

B. Sparse imaginary time grid

In this section, we examine the number of imaginary time grid points necessary to perform the Fourier transform ($\Sigma(i\tau) \rightarrow L$) accurately. This assessment is absolutely vital to the success of many approaches where evaluation of the self-energy on the time grid is the computation bottleneck.

To estimate the number of grid points necessary we performed calculations for atoms and molecules using different numbers of imaginary time points. While both atoms and molecules that we use here as test examples do not display different physics for a large range of temperatures due to the size of the gap present in these systems, they are very challenging examples since we strive to calculate electronic energy for very low temperatures near absolute zero (large value of inverse temperature $\beta = 100$). Consequently, our grid spacing has to be very small and the grid has to span significant energy window shown in Figure 1 thus requiring very many points if the uniform or power-law grids are used. For numerical Fourier transforms we used two different grids, a uniform grid and power-law grid as described below. For the ($\Sigma(i\tau) \rightarrow L$) transform, we used a modification of the power-law grid to compute a fixed number of Legendre coefficients. We have chosen 200 expansion coefficients since such a number of coefficients allows us to calculate the energy to μHa accuracy.

1. Uniform imaginary time grid

The grid points are uniformly spaced within the interval $[0, \beta]$ where the antiperiodic $G(i\tau)$ or $\Sigma(i\tau)$ is represented.

2. Power-law time grid

Since imaginary time self-energy is sharply peaked around endpoints (0 and $\pm\beta$) it is convenient to use non-uniformly spaced grids to represent it. A power-law grid⁴⁴ is constructed to be dense around endpoints and sparse between them where imaginary time self-energy is close to zero. The power-law grid is defined by two parameters: the power coefficient p and the uniform coefficient u . The first step in creating such a grid is placing points with the coordinates $\tau_j = \beta/2^j, j \in \{0, \dots, p-1\}$ starting from each endpoint and also placing a midpoint at $\beta/2$. Consequently, such a grid has $2p+1$ points. Then, each interval between power points is divided into $2u$ uniformly spaced subintervals.

3. ($\Sigma(i\tau) \rightarrow L$) transform with a power-law grid

We evaluated Legendre expansion coefficients employing only a fraction of the original power-law grid. We

kept number of power points fixed $p = 12$ and choose the number of uniform points as $u = 2^n$ where $n \in \{0, \dots, 5\}$. The resulting grid has $2u(p+1)+1$ imaginary time points that correspond to 53, 105, 209, 417 and 833 points for $n \in \{0, \dots, 5\}$ respectively.

Using the uniform, power-law grid and orthogonal polynomial transform, we evaluated the Matsubara self-energy $\Sigma(i\omega)$. In Figure 3, we show convergence for different grids. We set as our reference the self-energy obtained with 200 Legendre polynomials.

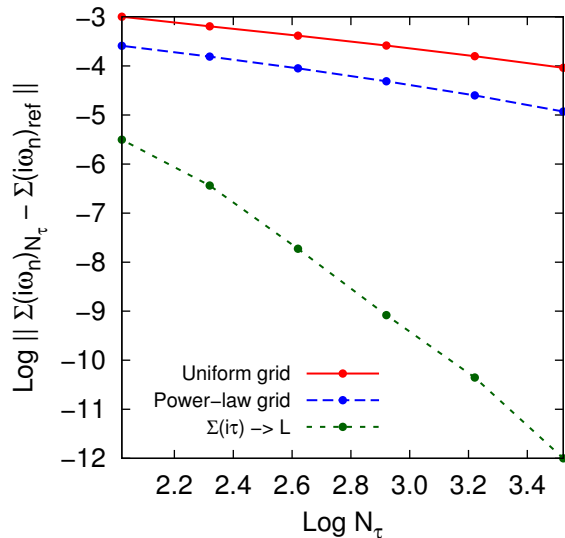


FIG. 3. Convergence of the self-energy $\Sigma(i\omega_n)$ as a function of number of imaginary time points.

As seen in Figure 3, the $(\Sigma(i\tau) \rightarrow L)$ and $(L \rightarrow \Sigma(i\omega))$ transforms converge much faster than the regular $(\Sigma(i\tau) \rightarrow \Sigma(i\omega))$ Fourier transform performed using a uniform or power-law grid.

III. SELF-CONSISTENT SECOND-ORDER GREEN'S FUNCTION THEORY USING ORTHOGONAL POLYNOMIAL TRANSFORM

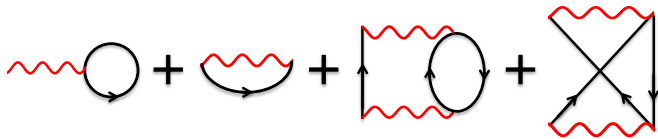


FIG. 4. GF2 is the second order approximation to the self-energy. It includes two first order self-energy diagrams (from left to right): Hartree (direct), Fock (exchange) and two second order self-energy diagrams: direct and exchange.

In this section, as an application to realistic calculations, we briefly describe the framework of the self-

consistent second-order Green's function theory (GF2) using an orthogonal polynomial transform.

GF2 employs the second-order approximation to the self-energy resulting in inclusion of all Feynman self-energy diagrams up to the second order, as shown in Figure 4. The first two diagrams are already included at mean-field level. Within spin-restricted GF2, the last two diagrams are translated into the following expression for the imaginary time self-energy

$$\Sigma_{ij}(i\tau_n) = - \sum_{klmnpq} G_{kl}^0(i\tau_n) G_{mn}^0(i\tau_n) G_{pq}^0(-i\tau_n) \times v_{imqk} (2v_{lpnj} - v_{nplj}), \quad (5)$$

where $G^0(i\tau_n)$ is the zeroth order imaginary time Green's function and v_{ijkl} are two-electron integrals defined as

$$v_{ijkl} = \int \int d\mathbf{r}_1 d\mathbf{r}_2 \phi_i^*(\mathbf{r}_1) \phi_j(\mathbf{r}_2) \frac{1}{r_{12}} \phi_k^*(\mathbf{r}_1) \phi_l(\mathbf{r}_2). \quad (6)$$

In GF2, as illustrated in Figure 2 for a general case, the calculation of the second-order self-energy according to eq 5 is done in the imaginary time domain while the Dyson equation from Figure 2 is much easier to solve in the frequency domain.

In our previous implementation, a typical molecular all electron GF2 calculation that involves both core and virtual orbitals may require many thousands of Matsubara frequencies N_ω making the total amount of storage necessary equal to $O(N_\omega n^2)$, where n is the number of orbitals. The imaginary time Green's function is represented by $O(N_\tau n^2)$ double precision numbers, where N_τ is the number of points of the imaginary time grid. Building the self-energy according to eq 5 scales as $O(N_\tau n^5)$, and despite that the self-energy calculation at any given imaginary time point is independent and can be made parallel, a large prefactor N_τ is slowing down calculations significantly even when using a power-law grid.

Since employing the orthogonal polynomial transform restricts the imaginary time grid even for the most difficult cases to fewer than 400 points, we implemented it as part of our algorithm. Here, we give a complete step-by-step modified algorithm description.

1. Start with Hartree-Fock (HF) reference solution (although starting from DFT reference is equally possible and advantageous for cases that are difficult to converge using HF) and build initial Matsubara Green's function in non-orthogonal AO basis according to:

$$\mathbf{G}_0(i\omega_n) = [(\mu + i\omega_n)\mathbf{S} - \mathbf{F}]^{-1}, \quad (7)$$

where \mathbf{S} is the overlap matrix, \mathbf{F} is the Fock matrix and μ is the chemical potential.

2. Perform discrete Fourier transform of $\mathbf{G}_0(i\omega_n)$ into its imaginary time counterpart $\mathbf{G}_0(i\tau)$. Alternatively, at this point, it is possible to avoid discrete

Fourier transform if one starts directly from the imaginary time HF Green's function constructed from HF orbital energies

$$G_{ij}^0(i\tau_n) = \theta(i\tau_n) (n(E_i) - 1) e^{-E_i i\tau_n} + \theta(-i\tau_n) n(E_i) e^{-E_i i\tau_n}, \quad (8)$$

where $\theta(x)$ is Heaviside step function, $E_i = \epsilon_i - \mu$ and $n(E_i) = 1/(e^{\beta E_i} + 1)$ is the Fermi distribution. Since the Green's function from eq 8 is constructed using MO orbital energies, it should be transformed to AO basis before proceeding to the next step.

3. Calculate the self-energy on the imaginary time grid according to eq 5. It is at this point where we first take advantage of Legendre polynomial representation of self-energy, since the Legendre representation allows us to use small imaginary time grids with only a fraction of points of the grid we used in our original implementation³⁶.
4. Obtain the Legendre expansion coefficients by performing an integration of the self-energy $\Sigma(i\tau)$ according to eq 2.
5. Build the imaginary frequency self-energy $\Sigma(i\omega)$ by performing a transform of Legendre coefficients according to eq 4.
6. Solve the Dyson equation to obtain an updated Green's function.
7. Find the chemical potential μ to ensure that a proper number of electrons is present in the system.
8. Calculate the density matrix and use it to update Fock matrix.
9. Go to point 6 and iterate until the density matrix and chemical potential μ stop to change.
10. Calculate the one-body energy as

$$E_{1b} = -\frac{1}{2} \sum_{\mu} \sum_{\nu} P_{\nu\mu} (t_{\mu\nu} + F_{\mu\nu}), \quad (9)$$

where $P_{\nu\mu} = -2G_{\nu\mu}(i\tau = \beta)$ is the correlated density matrix and the Fock matrix is evaluated using this correlated density matrix. The two-body energy can be evaluated using as

$$E_{2b} = -\frac{1}{\beta} \sum_{n=0}^{n_{freq}} \text{Tr}[G(i\omega_n)\Sigma(i\omega_n)], \quad (10)$$

for details see ref 45.

11. Transform $G(i\omega)$ to $G(i\tau)$ and go to step 3 and iterate until the total energy converges.

IV. RESULTS AND DISCUSSION

In this section, we provide results of atomic and molecular calculations with the above introduced GF2 algorithm. To assess the accuracy and efficiency of the algorithm described above, we performed several benchmark calculations with large basis sets using diffuse orbitals. These basis sets usually required the most extensive imaginary time grid and are necessary to reach quantitative accuracy and converge with basis set size.

Additionally, we also tested our algorithm on a few systems with transition metal atoms with ecp-sdd-DZ⁴⁶⁻⁴⁹ basis set containing pseudopotentials for inner shell electrons. We investigated systems with pseudopotentials since these are frequently used in solid state calculations and it is our interest to assess how compact the grids can become for such systems.

Our investigations can be divided into two groups evoking our original questions about (i) the size of the grid necessary to calculate the Legendre coefficients accurately and (ii) the compactness of the Legendre expansion.

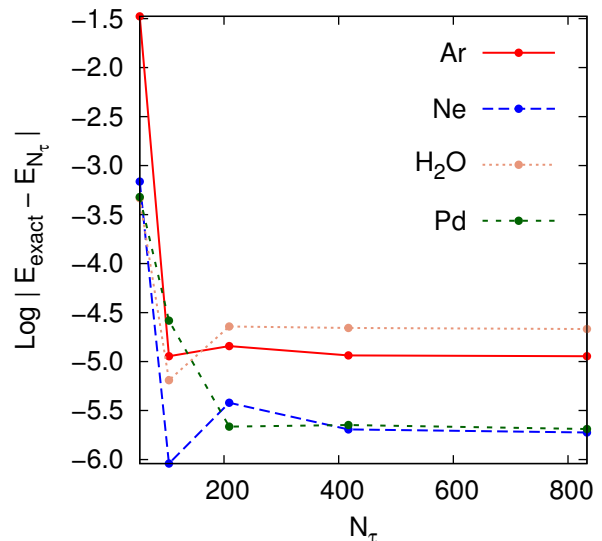


FIG. 5. Convergence of electron correlation energy with the size of imaginary time grid N_τ calculated for a few atoms and molecules.

A. Convergence of the electronic energy with respect to the grid size

We calculated the electronic correlation energy according to eq 10 for the grids defined in Section IIB3 and compared it to the one obtained using our previous GF2 implementation with sufficiently large imaginary time grids. Our previous implementation required at least an

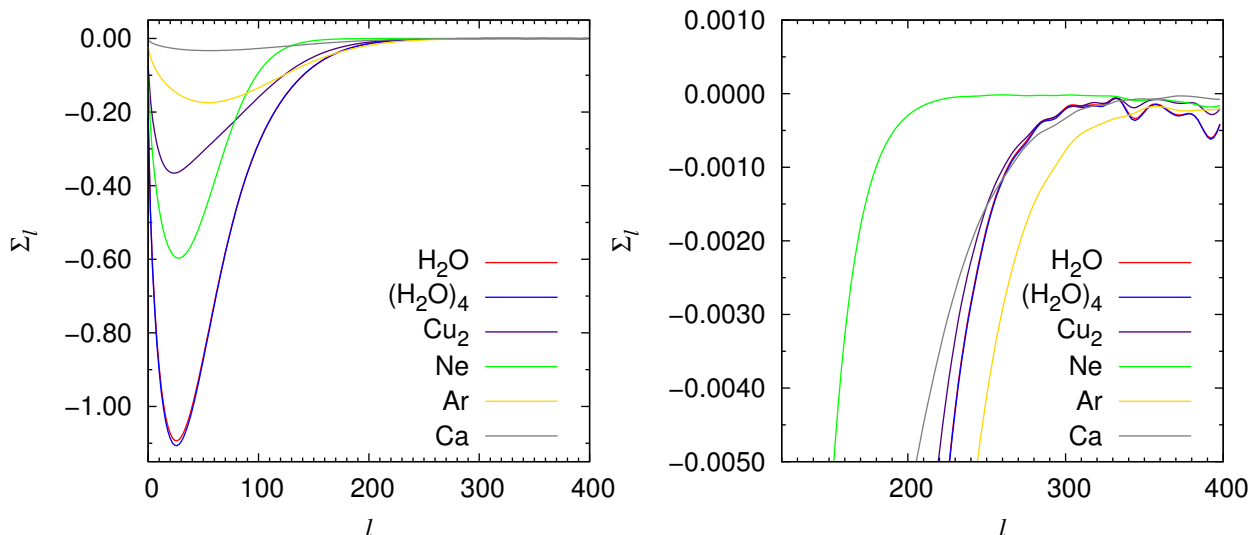


FIG. 6. Even coefficients of Legendre expansion of self-energy calculated using imaginary time grid consisting of 417 points for atoms and molecules. Left panel shows zoomed in region where $\Sigma^l \approx 0$ where Gibbs oscillations start to develop.

order of magnitude larger grids than the current one using the Legendre expansion.

In Figure 5, we plot the error in electronic correlation energy obtained by using different number of imaginary time points that are used to produce Legendre expansion of self-energy consisting of 200 expansion coefficients. Let us first note that using 200 Legendre coefficients results on average in 20 or less μHa error in the total energy, see Table I.

If we set the value of correlation energy using 200 Legendre polynomials as a reference then it is evident from Figure 5 that with only 104 imaginary time grid points an acceptable accuracy (less than 50 μHa from the exact answer) can be achieved. This is already far below the commonly accepted chemical accuracy of ≈ 1 kcal/mol. Using fewer than 100 grid points is not advisable since for 53 points for every examined case the accuracy was about 0.5 $m\text{Ha}$ away from the exact answer that is unacceptable in almost any quantum chemical calculation. For imaginary time grids with 209 and more points the accuracy reaches a plateau since for 200 Legendre coefficients a grid of 209 frequency points is sufficient to produce these coefficients with accuracy reaching numerical precision. If we desired to reach better accuracy than μHa level, then a larger number of the Legendre expansion coefficients should be employed in our calculation.

B. Compactness of the Legendre expansion

Next, we will study how the accuracy of our calculations depends on the number of terms in Legendre expansion of the self-energy. We fix the size of imaginary time grid to 417 points because, as it is seen from Fig-

TABLE I. Error in μHa of the total energy for different number of Legendre expansion coefficients for several atoms and molecules.

atom or molecule	l=200	l=100	l=40
He	0.09	0.05	-44.47
Be	0.30	0.02	-8.29
Ne	-1.05	-69.57	-177.23
Mg	0.50	-6.70	-6.28
Ar	-9.93	-28.53	697.07
Ca	-3.42	-7.54	401.17
H ₂ O ^a	-22.00	-99.99	9478.18
(H ₂ O) ₂ ^a	-27.26	372.33	21048.60
(H ₂ O) ₃ ^a	-53.20	47.81	29737.13
(H ₂ O) ₄ ^a	-71.21	63.47	39668.95
NH ₃ ^b	-7.12	-225.17	6953.89
C ₆ H ₆ ^b	-7.87	-668.08	28778.84
Cd	-2.27	-38.27	201.04
Cu ₂ ^c	-31.09	-151.26	6794.16
Pd	-2.25	-48.21	121.04
Ag ₂ ^d	-4.67	-36.86	658.88

^a Geometry was taken from ref 50.

^b Experimental geometries were taken from NIST Computational Chemistry Comparison and Benchmark Database⁵¹.

^c $d(\text{Cu-Cu})=3.63$ a. u.

^d $d(\text{Ag-Ag})=5.46$ a. u.

ure 5, this number of imaginary frequencies is sufficient to produce at least 200 accurate Legendre coefficients in the expansion of the self-energy.

First, we will look at values of expansion coefficients Σ_{00}^l determined by integrating self-energy according to eq 2. In Figure 6 we plotted even Legendre coefficients for a few atoms and molecules. Odd coefficients show very

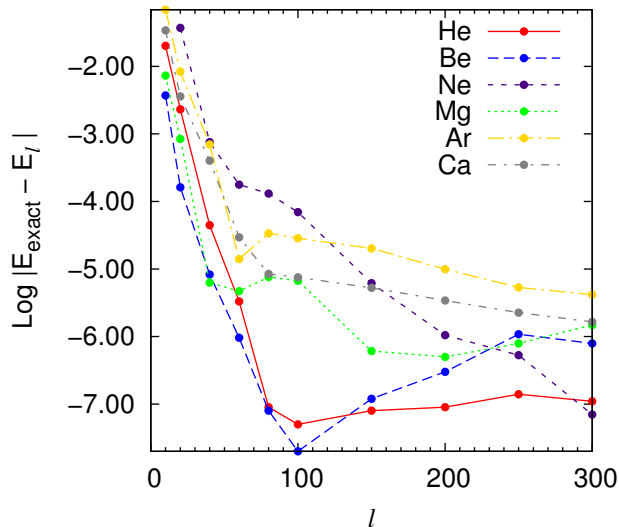


FIG. 7. Difference between the standard GF2 correlation energy and correlation energy obtained by using Legendre expansion of the self-energy for several closed-shell atoms with aug-cc-pVDZ basis set (cc-pVDZ basis set was used for Ca).

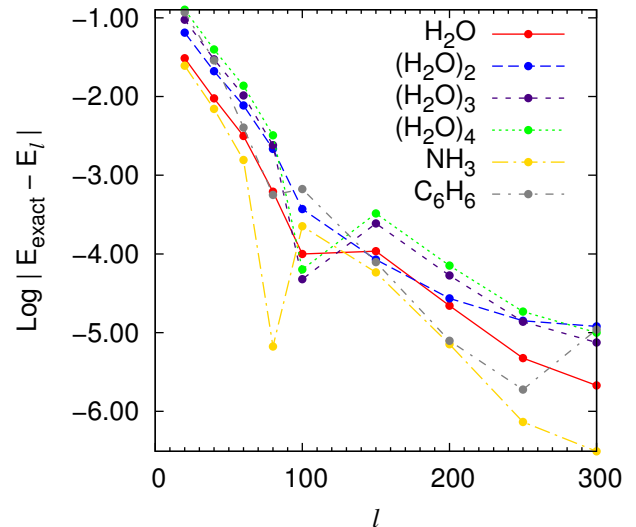


FIG. 9. Difference between the standard GF2 correlation energy and correlation energy obtained by using Legendre expansion of the self-energy for several small molecules with TZ basis set.

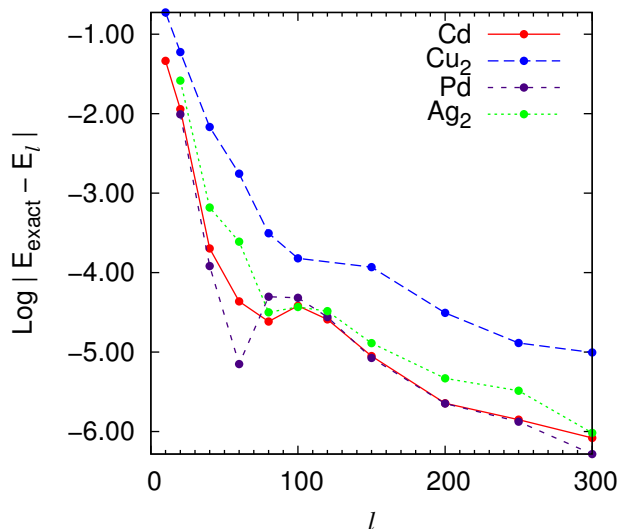


FIG. 8. Difference between the standard GF2 correlation energy and correlation energy obtained by using Legendre expansion of the self-energy for several transition metal atoms and diatomic clusters with ecp-sdd-DZ basis set.

similar behavior in almost all cases. As seen from the left panel of Figure 6, Legendre coefficients decay monotonically, converging to zero with the decay rate that is system-specific. For all cases studied in this work, we observe a fast decay of Legendre expansion coefficients used to represent the imaginary time self-energy. Thus, the Legendre polynomials form a compact representation

not only for Hubbard model³⁹ but also for atoms and molecules. Since realistic molecular systems have diffuse orbitals and span large energy spectrum an increase in the number of expansion terms in comparison to the Hubbard model is to be expected.

The right panel of Figure 6 shows a zoom in the region where the expansion coefficients are close to zero, $\Sigma_{00}^l = 0$. A closer look at the values of Σ_{00}^l reveals a numerical noise. This noise is known as Gibbs's oscillations⁵² and arises when too few imaginary time grid points are used to evaluate higher order Legendre coefficients. In order to prevent numerical noise buildup affecting very high orders of the Legendre expansion, one should truncate the expansion once oscillations are detected. Another method is to damp Gibbs oscillations by introducing an integral kernel function⁵². This option has been previously explored in the context of the Hubbard model⁴⁰. The particular choice of integral kernel function depends on several factors and is not convenient, especially if a black-box method is desired. Motivated by our aspiration to keep the self-energy as compact as possible, we took the first route and studied how the truncation of the Legendre expansion of the self-energy influences the accuracy of the method. The truncation of the expansion is unambiguous and the resulting self-energy is free from Gibbs oscillations. It is also worth mentioning that truncation criteria can be easily implemented and do not require any special care from the user and hence can be introduced as a part of any black-box computational package.

We performed calculations for our test set containing atoms and simple molecules truncating the Legendre series after various number of terms $\Sigma_{ij}^l = 0$ for $l > l_{\text{cut}}$.

Figures 7-9 show that only couple hundreds of Legendre expansion coefficients are necessary to yield very accurate results. All these results were calculated using 417 imaginary time points. In all cases very fast convergence was achieved and less than 100 Legendre polynomials were needed to converge correlation energy to 1 $m\text{Ha}$. We observe that for all atoms considered here the energy continues to converge to the exact one and about 200 Legendre polynomials are needed to recover it up to the μHa from the exact result. Similar observations can be made for calculations involving pseudopotentials and thus our method can be reliably applied to calculations of complex systems containing both transition metals and light atoms. A somewhat slower convergence was observed in the case of molecular calculations. In this case more than 200 but less than 300 Legendre polynomials were necessary to get within few μHa from the exact energy.

V. SUMMARY AND CONCLUSIONS

The frequency—time duality is present in many temperature-dependent methods and $G(i\tau)$ or $\Sigma(i\tau)$ can be transformed to $G(i\omega)$ or $\Sigma(i\omega)$ depending if handling the time or frequency object is more computationally advantageous. Both the frequency and time Green's functions have to be represented on a numerical grid, thus a small number of grid points is crucial for achieving computational efficiency.

While the construction of imaginary time grids is a well-studied problem and appears in Laplace-transformed Møller–Plesset (LT-MP2) perturbation theory, such grids are appropriate for the zero-temperature Green's function but cannot be employed to study the temperature-dependent Green's function.

In this paper, we have presented a method that makes transform between imaginary time and imaginary fre-

quency for temperature-dependent Green's function converge much faster with respect to the number of necessary imaginary time points than the traditional uniform and power-law grid. To achieve this goal we have used a combination of a very sparse power-law grid together with explicit transform based on a Legendre expansion of the self-energy. We have shown that to converge the Legendre coefficients necessary to perform the explicit transform we need an order of magnitude fewer imaginary time points that when doing the numerical Fourier transform.

Moreover, we have also shown that even for realistic systems in basis sets with a significant energy spread only a few hundred (200-300) of Legendre coefficients are necessary to reach the accuracy of μHa when compared with the fully converged result. Overall the orthogonal polynomial representation of self-energy offers fast, accurate, and less storage demanding solution for practical realistic calculations.

We have also applied such a representation of the self-energy to the GF2 method resulting in very accurate energies for atoms and molecules while using only a limited number of imaginary time grid points and only couple hundred (200-300) of Legendre expansion coefficients.

While at present no large scale realistic calculations are performed including temperature coming from the electronic effects, due to the increasing interest in new materials, we believe that such calculations will become important in the near future and identifying and overcoming major bottlenecks connected to the efficient representation of Green's function and self-energy in the imaginary time domain is an important step in this new direction.

ACKNOWLEDGMENTS

A. A. K., J. J. P, and D. Z. acknowledge support by DOE ER16391.

-
- ¹ A. D. Becke, *J. Chem. Phys.* **88**, 2547 (1988).
² C. W. Murray, N. C. Handy, and G. J. Laming, *Mol. Phys.* **78**, 997 (1993), <http://dx.doi.org/10.1080/00268979300100651>.
³ P. M. Gill, B. G. Johnson, and J. A. Pople, *Chem. Phys. Lett.* **209**, 506 (1993).
⁴ M. E. Mura and P. J. Knowles, *J. Chem. Phys.* **104**, 9848 (1996).
⁵ P. M. W. Gill and S.-H. Chien, *J. Comput. Chem.* **24**, 732 (2003).
⁶ J. Almlöf, *Chem. Phys. Lett.* **181**, 319 (1991).
⁷ M. Häser and J. Almlöf, *J. Chem. Phys.* **96**, 489 (1992).
⁸ A. F. Izmaylov and G. E. Scuseria, *Phys. Chem. Chem. Phys.* **10**, 3421 (2008).
⁹ B. Doser, D. S. Lambrecht, and C. Ochsenfeld, *Phys. Chem. Chem. Phys.* **10**, 3335 (2008).
¹⁰ D. Kats, D. Usvyat, and M. Schutz, *Phys. Chem. Chem. Phys.* **10**, 3430 (2008).
¹¹ P. Y. Ayala and G. E. Scuseria, *J. Chem. Phys.* **110**, 3660 (1999).
¹² M. Kaltak, J. Klimeš, and G. Kresse, *J. Chem. Theory Comput.* **10**, 2498 (2014), <http://dx.doi.org/10.1021/ct5001268>.
¹³ M. Bugeanu, R. Di Remigio, K. Mozgawa, S. S. Reine, H. Harbrecht, and L. Frediani, *Phys. Chem. Chem. Phys.*, (2015).
¹⁴ S. Nagy and J. Pipek, *Phys. Chem. Chem. Phys.*, (2015).
¹⁵ M. Zuzovski, A. Boag, and A. Natan, *Phys. Chem. Chem. Phys.*, (2015).
¹⁶ N. Scott Bobbitt, G. Schofield, C. Lena, and J. R. Chelikowsky, *Phys. Chem. Chem. Phys.*, (2015).
¹⁷ H.-J. Flad, G. Harutyunyan, and B.-W. Schulze, *Phys. Chem. Chem. Phys.*, (2015).
¹⁸ D. Chakraborty, S. Kar, and P. K. Chattaraj, *Phys. Chem. Chem. Phys.*, (2015).
¹⁹ A. Natan, *Phys. Chem. Chem. Phys.*, (2015).

- ²⁰ V. Khoromskaia and B. N. Khoromskij, *Phys. Chem. Chem. Phys.*, (2015).
- ²¹ E. A. Toivanen, S. A. Losilla, and D. Sundholm, *Phys. Chem. Chem. Phys.*, (2015).
- ²² T. L. Beck, *Phys. Chem. Chem. Phys.*, (2015).
- ²³ L. A. Espinosa Leal, A. Karpenko, M. A. Caro, and O. Lopez-Acevedo, *Phys. Chem. Chem. Phys.*, (2015).
- ²⁴ S. Mohr, L. E. Ratcliff, L. Genovese, D. Caliste, P. Boulanger, S. Goedecker, and T. Deutsch, *Phys. Chem. Chem. Phys.*, (2015).
- ²⁵ D. Baye and J. Dohet-Eraly, *Phys. Chem. Chem. Phys.*, (2015).
- ²⁶ X. Andrade, D. Strubbe, U. De Giovannini, A. H. Larsen, M. J. T. Oliveira, J. Alberdi-Rodriguez, A. Varas, I. Theophilou, N. Helbig, M. J. Verstraete, L. Stella, F. Nogueira, A. Aspuru-Guzik, A. Castro, M. A. L. Marques, and A. Rubio, *Phys. Chem. Chem. Phys.*, (2015).
- ²⁷ T. Yanai, G. I. Fann, G. Beylkin, and R. J. Harrison, *Phys. Chem. Chem. Phys.*, (2015).
- ²⁸ W. Hu, L. Lin, and C. Yang, *Phys. Chem. Chem. Phys.*, (2015).
- ²⁹ A. Nakata, D. R. Bowler, and T. Miyazaki, *Phys. Chem. Chem. Phys.*, (2015).
- ³⁰ J. S. Kottmann, S. Hofener, and F. A. Bischoff, *Phys. Chem. Chem. Phys.*, (2015).
- ³¹ E. Tsuchida, Y.-K. Choe, and T. Ohkubo, *Phys. Chem. Chem. Phys.*, (2015).
- ³² J. Kim, K. Hong, S. Choi, S.-Y. Hwang, and W. Youn Kim, *Phys. Chem. Chem. Phys.*, (2015).
- ³³ H. N. Rojas, R. W. Godby, and R. J. Needs, *Phys. Rev. Lett.* **74**, 1827 (1995).
- ³⁴ D. Foerster, P. Koval, and D. Sánchez-Portal, *J. Chem. Phys.* **135**, 074105 (2011).
- ³⁵ E. Gull, A. J. Millis, A. I. Lichtenstein, A. N. Rubtsov, M. Troyer, and P. Werner, *Rev. Mod. Phys.* **83**, 349 (2011).
- ³⁶ J. J. Phillips and D. Zgid, *J. Chem. Phys.* **140**, 241101 (2014).
- ³⁷ A. A. Kananenka, E. Gull, and D. Zgid, *Phys. Rev. B* **91**, 121111 (2015).
- ³⁸ J. J. Phillips, A. A. Kananenka, and D. Zgid, *J. Chem. Phys.* **142**, 194108 (2015).
- ³⁹ L. Boehnke, H. Hafermann, M. Ferrero, F. Lechermann, and O. Parcollet, *Phys. Rev. B* **84**, 075145 (2011).
- ⁴⁰ H. Li and D. Liang, arXiv:1205.2791 (2012).
- ⁴¹ M. Abramowitz and I. A. Stegun, *Handbook of Mathematical Functions with Formulas, Graphs, and Mathematical Tables* (Dover, New York, 1964).
- ⁴² L.-F. Arsenault, A. Lopez-Bezanilla, O. A. von Lilienfeld, and A. J. Millis, *Phys. Rev. B* **90**, 155136 (2014).
- ⁴³ W. Quan-Sheng, W. Yi-Lin, F. Zhong, and D. Xi, *Chin. Phys. Lett.* **30**, 090201 (2013).
- ⁴⁴ W. Ku and A. G. Eguiluz, *Phys. Rev. Lett.* **89**, 126401 (2002).
- ⁴⁵ A. L. Fetter and J. D. Walecka, *Quantum Theory of Many-Particle Systems* (Dover Publications, 2003).
- ⁴⁶ M. Dolg, U. Wedig, H. Stoll, and H. Preuss, *J. Chem. Phys.* **86**, 866 (1987).
- ⁴⁷ H. Stoll, P. Fuentealba, M. Dolg, J. Flad, L. v. Szentpály, and H. Preuss, *J. Chem. Phys.* **79**, 5532 (1983).
- ⁴⁸ D. Feller, *J. Comput. Chem.* **17**, 1571 (1996).
- ⁴⁹ K. L. Schuchardt, B. T. Didier, T. Elsethagen, L. Sun, V. Gurumoorthi, J. Chase, J. Li, and T. L. Windus, *J. Chem. Inf. Model.* **47**, 1045 (2007), <http://dx.doi.org/10.1021/ci600510j>.
- ⁵⁰ D. J. Wales and M. P. Hodges, *Chem. Phys. Lett.* **286**, 65 (1998).
- ⁵¹ “NIST Computational Chemistry Comparison and Benchmark Database,” NIST Standard Reference Database Number 101 Release 16a, August 2013, Editor: Russell D. Johnson III.
- ⁵² A. Weiße, G. Wellein, A. Alvermann, and H. Fehske, *Rev. Mod. Phys.* **78**, 275 (2006).